PERGAMON

International Journal of Heat and Mass Transfer 43 (2000) 3977–3990

International Journal of HEAT and MASS TRANSFER

www.elsevier.com/locate/ijhmt

Integral transform solutions of transient natural convection in enclosures with variable fluid properties

M.A. Leal[a], H.A. Machado[b], R.M. Cotta[c,*]

[a]*Comissão Nacional de Energia Nuclear — CNEN, Coordenação de Rejeitos Radioativos — COREJ, Rua General Severiano, 90 Botafogo, Rio de Janeiro, RJ 22294.900, Brazil*

[b]*Laboratório de Transmissão de Calor e Massa — LTCM, Mechanical Engineering Department, Universidade Federal de Uberlândia, DEEME-UFU, Campus Santa Mônica, Uberlândia, MG 38400-902, Brazil*

[c]*Laboratório de Transmissão e Tecnologia do Calor — LTTC, Mechanical Engineering Department, Universidade Federal do Rio de Janeiro, EE/COPPE/UFRJ, Cidade Universitária, Cx. Postal 68503, Rio de Janeiro, RJ 21945.970, Brazil*

Received 15 June 1999; received in revised form 17 January 2000

Abstract

This paper is aimed at the application of the Generalized Integral Transform Technique to the transient version of the classical differentially heated square cavity problem, considering both constant and variable fluid properties. The streamfunction-only formulation of the flow equations and the associated energy equation under laminar flow regime are employed in seeking a hybrid numerical–analytical solution to this natural convection problem. The computational procedure is carefully validated and a thorough convergence analysis is undertaken, yielding sets of reference results. The computed transient behavior of the coupled heat and fluid flow phenomena is compared to some previously reported results. The solution for variable fluid properties with partial Boussinesq approximation (density variation in the body force term only) is presented and compared with the constant properties results. Both models are investigated for different values of the Rayleigh number, from 10^3 to 10^5, and Prandtl number equal to 0.71.

1. Introduction

Natural convection inside cavities offers challenging test cases for the covalidation of numerical methods devised for the solution of coupled heat and fluid flow phenomena, governed by the continuity, the Navier–Stokes and the energy equations. The establishment of reliable benchmark results in both steady- and transient-state then becomes of major interest in allowing for critical comparisons among different scheme variants and computational implementation strategies.

In recent years, the so-called Generalized Integral Transform Technique (GITT) [1] has been successfully employed in the hybrid numerical–analytical solution of several classes of problems in diffusion and convection–diffusion, while being extended to the solution of the Navier–Stokes equations, either in isothermal flows or coupled to the energy equation formulated for the fluid motion [2–6].

The integral transform method, due to its hybrid numerical–analytical structure, offers the attractive feature of automatically controlling the global error in the computation, in a way similar to a purely

* Corresponding author. Tel.: +55-21-9988-6208; fax: +55-21-290-6626.

E-mail address: cotta@serv.com.ufrj.br (R.M. Cotta).

0017-9310/00/$ - see front matter
PII: S0017-9310(00)00023-5

Nomenclature

Cp	fluid specific heat (dimensionless without subscript)
g	gravity acceleration
k	fluid thermal conductivity (dimensionless)
L	cavity length and height
M_p, K_r	normalization integrals, Eqs. (11c) and (12c)
$N_{i,l}$	normalization integrals, Eq. (9)
NT	truncation order in temperature expansions
Nu	Nusselt number, Eqs. (23c–23e)
NV	truncation order in streamfunction expansions
Pr	Prandtl number ($=\nu_0/\alpha_0$)
Ra	Rayleigh number ($=g\beta(T_h-T_c)L^3/\alpha_0\nu_0$)
T	temperature (dimensionless)
$\bar{T}$	transformed temperature (dimensionless)
T^*	filtered temperature (dimensionless)
u	velocity component, x direction (dimensionless)
v	velocity component, y direction (dimensionless)
x	space coordinate (dimensionless)
y	space coordinate (dimensionless)
X_i, Y_l	eigenfunctions (streamfunction), Eqs. (6a,b) and (7a,b)
t	time (dimensionless)

Greek symbols

α	fluid thermal diffusivity
α_k, γ_q	reordered eigenvalues, (Eqs. (19a,b))
β	thermal expansion coefficient
β_p, λ_r	eigenvalues (temperature), Eqs. (11b) and 12(b)
ϕ_p, Γ_r	eigenfunctions (temperature), Eqs. (11a), (12a)
ψ	streamfunction (dimensionless)
$\bar{\psi}$	transformed streamfunction
μ, ν	absolute and kinematic viscosities (dimensionless without subscript)

Subscripts

k, q	reordered eigenquantities indices
h, c	hot and cold walls, respectively
0	property estimate at initial temperature, dimensional
$*$	dimensional variables (T_*, x_*, y_*, k_*, Cp_*, u_*, v_*, t_*, ψ_*, μ_*)

analytical approach. This aspect enables the essential confidence on the final converged results accuracy, making this type of approach particularly suitable for the confirmation and/or generation of benchmark results for different classes of problems in heat and fluid flow. Among various other contributions, of specific relevance to the application here considered, it is worth mentioning the integral transform solutions of the Navier–Stokes equations under the streamfunction-only formulation, for incompressible flow within cavities and channels [2,3] and natural convection under the Boussinesq approximation inside rectangular enclosures for both steady and transient states [4,5]. In addition, natural convection within porous rectangular enclosures was accurately solved through the same integral transform approach [6].

In 1983, De Vahl Davis [7] provided the first set of benchmark solutions for the steady natural convection in a enclosed square cavity with differentially heated vertical walls and insulated top and bottom walls, utilizing a second-order finite differences method and the Richardson extrapolation scheme. Following this pioneering work, different solution strategies have been reported in the literature. Among the most relevant works to our present objectives, one can cite Saitoh and Hirose [8], who utilized a non-conservative fourth-order finite differences approach in 1989, Hortmann et al. [9], who have made use of the finite volume method in 1990, and Lé Queré [10], who employed a pseudo-spectral Chebyshev algorithm to provide accurate solutions to values of Rayleigh number from 10^6 to 10^8, in 1991.

In contrast with steady natural convection, transient analysis of natural convection in a cavity has received much less attention in the literature, despite its scientific and technological relevance. A brief literature review includes the contributions of Wilkes and Churchill [11] in 1966, who provided a pioneering transient analysis using an implicit alternating direction (ADI) finite difference method, Patterson and Imberger [12], in a classical work, who used a simple scale analysis to give some insight into the possible transient behavior and obtained a number of numerical solutions using a modified version of the finite difference method proposed by Chorin [13]. More recently, Sai et al. [14] presented solutions for the transient problem in the Rayleigh number range of 10^3–10^6 by the application of the finite element method based on the first-order projection scheme, which is an extension of Chorin's algorithm. Ramaswamy et al. [15] applied a

semi-implicit projection-type finite element method to perform two numerical tests, oscillatory cavity flow with heat transfer and transient buoyancy-driven flow in a square cavity.

Parallel to these research efforts, and also in recent years, the influence of the fluid properties variation with temperature has appeared as an important aspect to be analyzed in this class of problems. The well-known Boussinesq approximation has been extensively employed, but very little research has been undertaken to inspect the influence of variable thermophysical properties in the flow structure, with or without the Boussinesq simplification. Among other researches of relevance to our present purposes, Bergles [16] presented correlation formulae to compute the influence of each property (viscosity and conductivity) for forced convection in tubes, considering incompressible flow. Gray and Giorgini [17] studied the limit of application of the Boussinesq approximation to external flows of water and air, using two orders of approximation: strict and extended. They presented also graphics to indicate accurate limits to those hypothesis. The stability and the limits of the Boussinesq approximation were also the subject in the works of Graham [18] and Spradley and Churchill [19], both using the finite difference method to compute the lid-driven cavity problem for a compressible fluid with variable properties. Suslov and Paollucci [20] reproduced and extended the results of these works, aimed at finding the critical Rayleigh number, and at showing the presence of two regimen of instability, one of them due to the non-Boussinesq effects. Yu et al. [21] tried to present a benchmark for the compressible problem (the lid-driven cavity), using finite element analysis, and handling the common limitations of this method when applied to low-Mach number compressible flows. Finally, Zhong et al. [22] revised the work of Graham [18], centering their study in the validity of the Boussinesq approximation. They found a more strict limit than the one presented in [17], despite of the good agreement achieved for Nusselt number calculations.

Here, the results obtained for variable properties will be inspected within and outside the limits predicted in [22], considering variations of dynamic viscosity, thermal conductivity, specific heat and density in the body force term only. Thus, maintaining the Boussinesq approximation, the temperature variation effects, on the flow structure, of all other thermophysical properties will be analyzed. We first reproduce through integral transformation, the transient natural convection solutions under the Boussinesq approximation and constant properties to reconfirm some previously reported reference results, for which there is an evident lack of formal confidence on their global accuracy control. The method is then validated and the solutions are compared with those obtained for the variable properties situation, when the very desirable hybrid characteristics of the GITT are explored in a situation of marked non-linear effects, in automatically controlling the global error in the simulation.

2. Problem formulation

The problem to be solved corresponds to the two-dimensional transient form of the coupled continuity, Navier–Stokes and energy equations, applied to a fluid filled square cavity, where the density is considered constant throughout except in the buoyancy term, with the horizontal walls insulated, and a prescribed temperature difference applied between the two vertical walls. The governing equations, presented for variable physical properties, are the vorticity transport equation in the streamfunction-only formulation, and the associated energy equation, which in dimensionless form are given by:

$$\frac{\partial}{\partial t}\left(\nabla^2\psi\right)+\frac{\partial\psi}{\partial y}\frac{\partial\left(\nabla^2\psi\right)}{\partial x}-\frac{\partial\psi}{\partial x}\frac{\partial\left(\nabla^2\psi\right)}{\partial y}$$
$$=Pr_0\left[\mu\nabla^4\psi+2\frac{\partial\mu}{\partial y}\nabla^2\left(\frac{\partial\psi}{\partial y}\right)+2\frac{\partial\mu}{\partial x}\nabla^2\left(\frac{\partial\psi}{\partial x}\right)\right.$$
$$\left.+4\frac{\partial^2\mu}{\partial x\partial y}\frac{\partial^2\psi}{\partial x\partial y}+\left(\frac{\partial^2\mu}{\partial y^2}-\frac{\partial^2\mu}{\partial x^2}\right)\left(\frac{\partial^2\psi}{\partial y^2}-\frac{\partial^2\psi}{\partial x^2}\right)\right]$$
$$-Ra_0Pr_0\frac{\partial T}{\partial x}\quad 0<x<1,\,0<y<1,\,t>0 \tag{1a}$$

$$\frac{\partial T}{\partial t}+\frac{\partial\psi}{\partial y}\frac{\partial T}{\partial x}-\frac{\partial\psi}{\partial x}\frac{\partial T}{\partial y}$$
$$=\frac{1}{\rho_0 Cp_0}\left(k\nabla^2T+\frac{\partial k}{\partial x}\frac{\partial T}{\partial x}+\frac{\partial k}{\partial y}\frac{\partial T}{\partial y}\right) \tag{1b}$$
$$0<x<1,\,0<y<1,\,t>0$$

with initial and boundary conditions

$$T(x,y,0)=\psi(x,y,0);\quad 0\le x\le 1,\,0\le y\le 1 \tag{2a,b}$$

$$T=1;\quad \psi=\frac{\partial\psi}{\partial x}=0;\quad x=0 \tag{2c–e}$$

$$T=0;\quad \psi=\frac{\partial\psi}{\partial x}=0;\quad x=1 \tag{2f–h}$$

$$\frac{\partial T}{\partial y}=0;\quad \psi=\frac{\partial\psi}{\partial y}=0;\quad y=0 \tag{2i–k}$$

$$\frac{\partial T}{\partial y}=0;\quad \psi=\frac{\partial\psi}{\partial y}=0;\quad y=1 \tag{2l–n}$$

where the reference Rayleigh and Prandtl numbers are defined as:

$$Ra_0 = \frac{g\beta(T_h - T_c)L^3}{\alpha_0 \nu_0} \quad \text{and} \quad Pr_0 = \frac{\mu_0 Cp_0}{k_0} \tag{3a,b}$$

and the remaining dimensionless variables are given by:

$$\psi = \frac{\psi_*}{\alpha_0}; \quad t = \frac{\alpha_0}{L^2} t_*; \quad x = \frac{x_*}{L}; \quad y = \frac{y_*}{L};$$
$$T = \frac{T_* - T_c}{T_h - T_c}; \quad \mu = \frac{\mu_*}{\mu_0}; \quad k = \frac{k_*}{k_0}; \tag{4a–h}$$
$$Cp = \frac{Cp_*}{Cp_0}$$

where the subscript "$*$" identifies the dimensional variables, the subscript "0" denotes the property estimate at the initial temperature, L is the dimension of the cavity, α is the fluid thermal diffusivity, μ is the variable kinematic viscosity, k is the variable thermal conductivity, Cp is the variable specific heat, T_h is the hot wall temperature, T_c is the cold wall temperature, g is the gravity acceleration and β is the fluid volumetric expansion coefficient.

3. Solution methodology

The first step in the solution procedure is the filtering strategy to enhance convergence of the eigenfunction expansions, by making the boundary conditions homogeneous. The simplest choice of a filtering solution for the temperature field is extracted from the steady pure conduction problem:

$$T(x, y, t) = T^*(x, y, t) + T_F(x) \tag{5a}$$

where the filter is written as:

$$T_F(x) = 1 - x \tag{5b}$$

More refined filtering could be proposed, for instance, by considering the transient version of the conduction problem, but the simple expression above suffices for our present needs.

The initial conditions for the filtered potentials are then rewritten as:

$$T^*(x, y, 0) = x - 1, \quad \psi(x, y, 0) = 0; \quad 0 \le x \le 1 \quad \text{and} \quad 0 \le y \le 1 \tag{5c,d}$$

and we should now seek a solution for the filtered temperature distribution, $T^*(x, y, t)$

The next step is the selection of the eigenfunctions basis in each direction, x and y, for each individual potential, ψ and T^*. Following previous developments [2–5], the streamfunction eigenvalue problems yield the following eigenfunctions in each coordinate:

$$X_i(x) = \begin{cases} \cos \varphi_i(x - 1/2) \sec(\varphi_i/2) - \cosh \varphi_i(x - 1/2) \\ \operatorname{sech}(\varphi_i/2); \quad \text{for } i = 1, 3, 5, \ldots \\ \sin \varphi_i(x - 1/2) \csc(\varphi_i/2) - \sinh \varphi_i(x - 1/2) \\ \operatorname{csch}(\varphi_i/2); \quad \text{for } i = 2, 4, 6, \ldots \end{cases} \tag{6a,b}$$

and

$$Y_\ell(y) = \begin{cases} \cos \varphi_\ell(y - 1/2) \sec(\varphi_\ell/2) - \cosh \varphi_\ell(y - 1/2) \\ \operatorname{sech}(\varphi_\ell/2); \quad \text{for } \ell = 1, 3, 5, \ldots \\ \sin \varphi_\ell(y - 1/2) \csc(\varphi_\ell/2) - \sinh \varphi_\ell(y - 1/2) \\ \operatorname{csch}(\varphi_\ell/2); \quad \text{for } \ell = 2, 4, 6, \ldots \end{cases} \tag{7a,b}$$

where the eigenvalues φ_i (or φ_ℓ) are the same in both directions x and y, and obtained from:

$$\tanh \frac{\varphi_{i,\ell}}{2} = \begin{cases} -\tan(\varphi_{i,\ell}/2) & \text{for } i \text{ and } \ell = 1, 3, 5, \ldots \\ \tan(\varphi_{i,\ell}/2) & \text{for } i \text{ and } \ell = 2, 4, 6, \ldots \end{cases} \tag{8a,b}$$

and the normalization integrals N_i and N_ℓ are found to be, in this special case:

$$N_{i,\ell} = 1; \quad \text{for } i \text{ and } \ell = 1, 2, 3, \ldots \tag{9}$$

The normalized eigenfunctions $\tilde{X}_i(x)$ and $\tilde{Y}_\ell(y)$ are then defined by:

$$\tilde{X}_i(x) = \frac{X_i(x)}{N_i^{1/2}}; \qquad \tilde{Y}_\ell(y) = \frac{Y_\ell(y)}{N_\ell^{1/2}} \tag{10a,b}$$

The eigenfuctions associated with the temperature problem in the x direction are given by:

$$\phi_p(x) = \sin \beta_p x; \quad \text{for } p = 1, 2, 3, \ldots \tag{11a}$$

with the eigenvalues and norms;

$$\beta_p = p\pi; \quad \text{for } p = 1, 2, 3, \ldots \tag{11b}$$

$$M_p = 1/2; \quad \text{for } p = 1, 2, 3, \ldots \tag{11c}$$

while in the y direction the temperature eigenvalue problem is solved as:

$$\Gamma_r = \cos \lambda_r y; \quad \text{for } r = 1, 2, 3, \ldots \tag{12a}$$

with eigenvalues:

$$\lambda_r = (r - 1)\pi; \quad \text{for } r = 1, 2, 3, \ldots \tag{12b}$$

and norms:

$$K_r = \begin{cases} 1; & \text{for } (r-1) = 0 \\ 1/2; & \text{for } (r-1) \neq 0 \end{cases} \tag{12c}$$

The normalized eigenfunctions $\tilde{\phi}_p(x)$ and $\tilde{\Gamma}_r(y)$ are defined as:

$$\tilde{\phi}_p(x) = \frac{\phi_p(x)}{M_p^{1/2}}; \quad \tilde{\Gamma}_r(y) = \frac{\Gamma_r(y)}{K_r^{1/2}} \tag{13a,b}$$

Following the formalism in the generalized integral transform technique, the double transformation for the streamfunction field in the x and y directions is obtained from the integral transform pairs below:

$$\bar{\psi}_{i\ell}(t) = \int_0^1 \int_0^1 \tilde{Y}_\ell(y)\tilde{X}_i(x)\psi(x, y, t)\,\mathrm{d}x\,\mathrm{d}y; \quad \text{transform} \tag{14a}$$

$$\psi(x, y, t) = \sum_{\ell=1}^{\infty}\sum_{i=1}^{\infty} \tilde{Y}_\ell(y)\tilde{X}_i(x)\bar{\psi}_{i\ell}(t); \quad \text{inverse} \tag{14b}$$

Similarly, for the temperature field in the x and y directions:

$$\bar{T}_{pr}(t) = \int_0^1 \int_0^1 \tilde{\Gamma}_r(y)\tilde{\phi}_p(x)T^*(x, y, t)\,\mathrm{d}x\,\mathrm{d}y; \quad \text{transform} \tag{15a}$$

$$T^*(x, y, t) = \sum_{r=1}^{\infty}\sum_{p=1}^{\infty} \tilde{\Gamma}_r(y)\tilde{\phi}_p(x)\bar{T}_{pr}(t); \quad \text{inverse} \tag{15b}$$

Applying the double transformations ((14a) and (15a)) in the streamfunction problem and in the temperature problem, respectively, produces the infinite coupled ODE system below:

$$\sum_{j=1}^{\infty}\sum_{m=1}^{\infty} E_{i\ell jm}\frac{\mathrm{d}\bar{\psi}_{jm}(t)}{\mathrm{d}t} = F_{i\ell}(t) \tag{16a}$$

$$\frac{\mathrm{d}\bar{T}_{pr}(t)}{\mathrm{d}t} = G_{pr}(t) \tag{16b}$$

The same transformation procedure is operated on the initial conditions, providing:

$$\bar{\psi}_{i\ell}(0) = 0 \quad \text{and} \quad \bar{T}_{pr}(0) = H_{pr} \tag{16c,d}$$

The coefficients above are integrals of the related eigenfunctions, given by:

$$E_{i\ell jm} = \int_0^1 \tilde{X}_i(x)\tilde{X}_j''(x)\,\mathrm{d}x \int_0^1 \tilde{Y}_\ell(y)\tilde{Y}_m(y)\,\mathrm{d}y + \int_0^1 \tilde{X}_i(x)\tilde{X}_j(x)\,\mathrm{d}x \int_0^1 \tilde{Y}_\ell(y)\tilde{Y}_m''(y)\,\mathrm{d}y \tag{17a}$$

$$F_{i\ell}(t) = \int_0^1 \int_0^1 \tilde{X}_i(x)\tilde{Y}_\ell(y)\left\{\frac{\partial\psi}{\partial x}\frac{\partial\left(\nabla^2\psi\right)}{\partial y} - \frac{\partial\psi}{\partial y}\frac{\partial\left(\nabla^2\psi\right)}{\partial x} + Pr_0[\mu\nabla^4\psi + 2\frac{\partial\mu}{\partial y}\nabla^2\left(\frac{\partial\psi}{\partial y}\right) + 2\frac{\partial\mu}{\partial x}\nabla^2\left(\frac{\partial\psi}{\partial x}\right) + 4\frac{\partial^2\mu}{\partial x\partial y}\frac{\partial^2\psi}{\partial x\partial y} + \left(\frac{\partial^2\mu}{\partial y^2} - \frac{\partial^2\mu}{\partial x^2}\right) \times \left(\frac{\partial^2\psi}{\partial y^2} - \frac{\partial^2\psi}{\partial x^2}\right)] - Ra_0 Pr_0\frac{\partial T}{\partial x}\right\}\mathrm{d}y\,\mathrm{d}x \tag{17b}$$

$$G_{pr}(t) = \int_0^1 \int_0^1 \tilde{\phi}_p(x)\tilde{\Gamma}_r(y)\left\{\frac{\partial\psi}{\partial x}\frac{\partial T}{\partial y} - \frac{\partial\psi}{\partial y}\frac{\partial T}{\partial x} + \frac{1}{\rho_0 Cp_0}\left(k\nabla^2 T + \frac{\partial k}{\partial x}\frac{\partial T}{\partial x} + \frac{\partial k}{\partial y}\frac{\partial T}{\partial y}\right)\right\}\mathrm{d}y\,\mathrm{d}x \tag{18a}$$

$$H_{pr} = \int_0^1 \int_0^1 \tilde{\Gamma}_r(y)\tilde{\phi}_p(x)(x-1)\,\mathrm{d}y\,\mathrm{d}x \tag{18b}$$

where $E_{i\ell jm}$ and H_{pr} are analytically obtained through symbolic manipulation packages [23], and $F_{i\ell}(t)$ and $G_{pr}(t)$ are obtained through numerical integration at each internal step of the ODE system solution.

Eqs. (16) form an infinite system of coupled nonlinear ODEs, to be solved for the transformed potentials, $\bar{\psi}_{i\ell}$ and $\bar{T}_{pr}$. From a computational point of view, only a truncated version of such nested summations can be actually evaluated. However, the plain truncation of these series, individually, to a certain prescribed finite order, is certainly not an efficient approach. In this way, some still important information to the final result can be disregarded, while other terms are accounted for that have essentially no contribution to convergence in the relative accuracy required. Therefore, for an efficient computation of these expansions, the infinite multiple summations should first be converted to a single sum representation, with the appropriate reordering of terms, according to their individual contribution to the final numerical result. Then, one would be able to evaluate a minimum number of eigenvalues and related derived quantities, as many as required to reach the user prescribed accuracy

target. This aspect is even more evident when the computational costs can be markedly reduced through this reordering of terms, which then represents a reduction on the number of ordinary differential equations to be solved numerically in the transformed system. Since the final solution is not, of course, known a priori, the parameter which shall govern this reordering scheme must be chosen with care, and proved to be a good choice. Once the ordering is completed, the remaining of the computational procedure becomes as straightforward and cost-effective as in the one-dimensional case. It is noticeable that the most common choice of ordering strategy, based on the argument of the dominating exponential term, although not always in a monotonic fashion, offers a good compromise between the overall convergence enhancement and simplicity in use. However, individual applications may require more elaborate reordering that accounts for the influence of nonlinear source terms in the ODE system.

The ordering scheme for multidimensional eigenfunction expansions employed is described in more detail in [24,25]. Here, the criteria selected for the ordering procedure involves the summation of the eigenvalues in each direction, or:

$$\alpha_k^4 = \varphi_{i(k)}^4 + \varphi_{\ell(k)}^4 \quad \text{and} \quad \gamma_q^2 = \beta_{p(q)}^2 + \lambda_{r(q)}^2 \tag{19a,b}$$

Then, the indices i and ℓ related to the streamfunction expansion are reorganized into the single index k, while the indices p and r for the temperature expansion are collapsed into the new index q. The associated double sums are then rewritten as $\sum_{j=1}^{\infty}\sum_{m=1}^{\infty} \rightarrow \sum_{n=1}^{\infty}$.

System (16) is then rewritten as:

$$\sum_{n=1}^{\infty} E_{kn} \frac{\mathrm{d}\bar{\psi}_n}{\mathrm{d}t} = F_k(t) \tag{20a}$$

$$\frac{\mathrm{d}\bar{T}_q}{\mathrm{d}t} = G_q(t) \tag{20b}$$

with initial conditions,

$$\bar{\psi}_k(0) = 0 \quad \text{and} \quad \bar{T}_q(0) = H_q \tag{20c,d}$$

System (20) above is now in the appropriate format for numerical solution. The expansions are then truncated to NV and NT terms, respectively, for the streamfunction and temperature fields, where the truncation orders are automatically selected along numerical integration of the ODE system so as to reach the user requested accuracy target, and the coefficients $F_k(t)$ and $G_q(t)$ are numerically evaluated at each step of the solution process.

Subroutine DIVPAG form the IMSL Library [26] is employed as the initial value problem solver, once system (20) is rewritten in the following form:

$$\boldsymbol{A}\boldsymbol{Y}' = f(\boldsymbol{Y}, t) \tag{21a}$$

$$\boldsymbol{Y}(0) = \boldsymbol{Y}_0 \tag{21b}$$

where the solution vector is given by:

$$\boldsymbol{Y} = \left\{\bar{\psi}_1(t), \ldots, \bar{\psi}_{NV}(t), \bar{T}_1(t), \ldots, \bar{T}_{NT}(t)\right\}^{\mathrm{T}} \tag{22}$$

System (21) is composed of $NV+NT$ ODEs, which are likely to experience high stiffness ratios. However, Gear's method implemented in subroutine DIVPAG [26] is capable of handling such situations, offering an automatic accuracy control scheme.

Quantities of practical interest are then readily obtained from the analytic inversion formulae, such as, the horizontal and vertical velocity components:

$$u = \sum_{k=1}^{NV} \tilde{X}_i(x) \frac{\mathrm{d}\tilde{Y}_\ell(y)}{\mathrm{d}y} \bar{\psi}_{i\ell}(t) \quad \text{and}$$
$$v = -\sum_{k=1}^{NV} \frac{\mathrm{d}\tilde{X}_i(x)}{\mathrm{d}x} \tilde{Y}_\ell(y) \bar{\psi}_{i\ell}(t) \tag{23a,b}$$

The maximum (or minimum) local Nusselt number at the hot wall ($x = 0$), is determined from the expression below:

$$Nu_{\mathrm{hot}} = -k(T) \left.\frac{\partial T}{\partial x}\right|_{x=0} \tag{23c}$$

the average Nusselt number at any x cross-section,

$$Nu_{\mathrm{av}} = \int_0^1 \left[u(x, y, t) T(x, y, t) - k(T) \frac{\partial T(x, y, t)}{\partial x} \right] \mathrm{d}y \tag{23d}$$

and the global Nusselt number across the cavity:

$$Nu_g = \int_0^1 Nu_{\mathrm{av}} \, \mathrm{d}x \tag{23e}$$

The integrations required in Eqs. (23d and 23e) are numerically performed by making use of the appropriate subroutines in the IMSL library [26].

4. Results and discussion

Two independent Fortran codes were built and implemented on a PC-PENTIUM II 200 MHz, where the user prescribed relative error criteria was selected to be either 10^{-5} or 10^{-4}, specialized, respectively, for the constant and variable properties cases. The code for constant properties was specially useful in validating the more general one, since in that case all the related integrals could be performed analytically, by employ-

Table 1
Values of θ_0 for each case studied

Ra	Boussinesq region	Limit (22)	Non-Boussinesq region
10^3	0.0101	0.1307	0.5
10^4	0.0101	0.2288	0.5
10^5	0.0101	0.4030	0.8

ing a symbolic manipulation system [23]. Three values of the Rayleigh number, equal to 10^3, 10^4 and 10^5, were analyzed, in both situations, for an air-filled square cavity ($Pr = 0.71$). Results are presented and compared for different times of interest during the transient process, in terms of velocity components, dimensionless temperature, local and average Nusselt numbers. Also, some steady-state results under the Boussinesq approximation have been compared with previously reported results. To evaluate the numerical integrals that define the coefficients $F_k(t)$ $G_q(t)$, up to 40 points had been used in Gaussian quadrature, and the convergence of this numerical procedure was carefully examined [27]. The functions employed to represent the fluid physical properties variation with temperature, provided by Zhong et al. [22] in dimensionless form, are written as:

$$\mu(T) = \frac{14.58 \times 10^{-7} T^{3/2}}{110.4 + T} \tag{24a}$$

$$k(T) = \frac{2.6483 \times 10^{-3} T^{3/2}}{T + 245.4 \times 10^{-(12/T)}} \tag{24b}$$

$$Cp(T) = 9898.24 - 0.3316T + 0.2025 \times 10^{-3} T^2 \tag{24c}$$

The limit of validity for the Boussinesq approximation is proposed by Zhong et al. [22] as:

$$\theta_0 = 0.0244 Ra^{0.243} \tag{25a}$$

where:

$$\theta_0 = \frac{T_h - T_c}{T_c} \tag{25b}$$

Thus, three distinct situations of variable properties are analyzed in relation to the Boussinesq hypothesis in order to compare the physical phenomena behavior in each one. The first one, within the proposed limit of the Boussinesq approximation, corresponds to a little difference between the hot and cold temperature walls ($\Delta T \approx 1$ K), the second one for an equivalent difference at the above theoretical limit and, finally, for a considerable difference between the cavity walls temperatures ($\Delta T \gg 1$ K), as illustrated in Tables 1 and 2.

Firstly, a set of comparisons was performed under the Boussinesq formulation with constant thermophysical properties against previously reported numerical results [14], for both the temperature and vertical velocity component (v) distributions. Fig. 1(a)–(c) illustrate such comparisons for all three cases, $Ra = 10^3$, 10^4 and 10^5, respectively, at the cavity midplane ($y = 1/2$). The overall agreement is quite reasonable to the graphic scale within the transient region. Some more noticeable deviations were identified as the time increases, probably due to some error propagation effect in the purely numerical solution of [14].

Table 2
Values of ΔT as function of θ_0

θ_0	ΔT (K)
0.0101	3.03
0.1307	39.21
0.2288	68.64
0.4030	120.90
0.5	150.00
0.8	240.00

Table 3 brings some comparisons of the present integral transform solutions for the transient constant properties formulation, when steady-state is attained, against previously reported results, obtained through different discrete approaches as in [14,15], as well as with the integral transform solution of the actual elliptic steady-state formulation of [4,7]. Values of interest such as the streamfunction modulus at the center of the cavity, $|\psi_{MED}|$, the maximum streamfunction modulus at the cavity $|\psi_{MAX}|$ (at $x = 0.855$ and $y = 0.601$ positions for $Ra = 10^5$), and the maximum vertical velocity component at the cavity midplane ($y = 1/2$), as in Ref. [7], are analyzed.

It is important to recall that the steady-state results from the present work, as well as the results presented by Sai at al. [14], have been obtained making use of the fully transient formulation in order to reproduce the transient behavior of the heat and fluid flow phenomena. Ramaswamy et al. [15] took advantage of the transient formulation but only reported steady-state solutions. For $Ra = 10^3$ the major difference between De Vahl Davis benchmark solutions [7] and the other proposed results is of 1.29% on the vertical velocity component supplied by [14]. For $Ra = 10^4$ the solutions appear to be more coincident, with the major difference among [7] and the other results being of 0.55% on the streamfunction modulus supplied in [15]. Finally, for $Ra = 10^5$, some scattering among the proposed solutions becomes more evident, while the major difference between the various proposed results and [7] is of 1.5% on the maximum streamfunction modulus $|\psi_{MAX}|$ supplied by Ramaswamy et al. [15]; also the difference of 1.33% between the vertical vel-

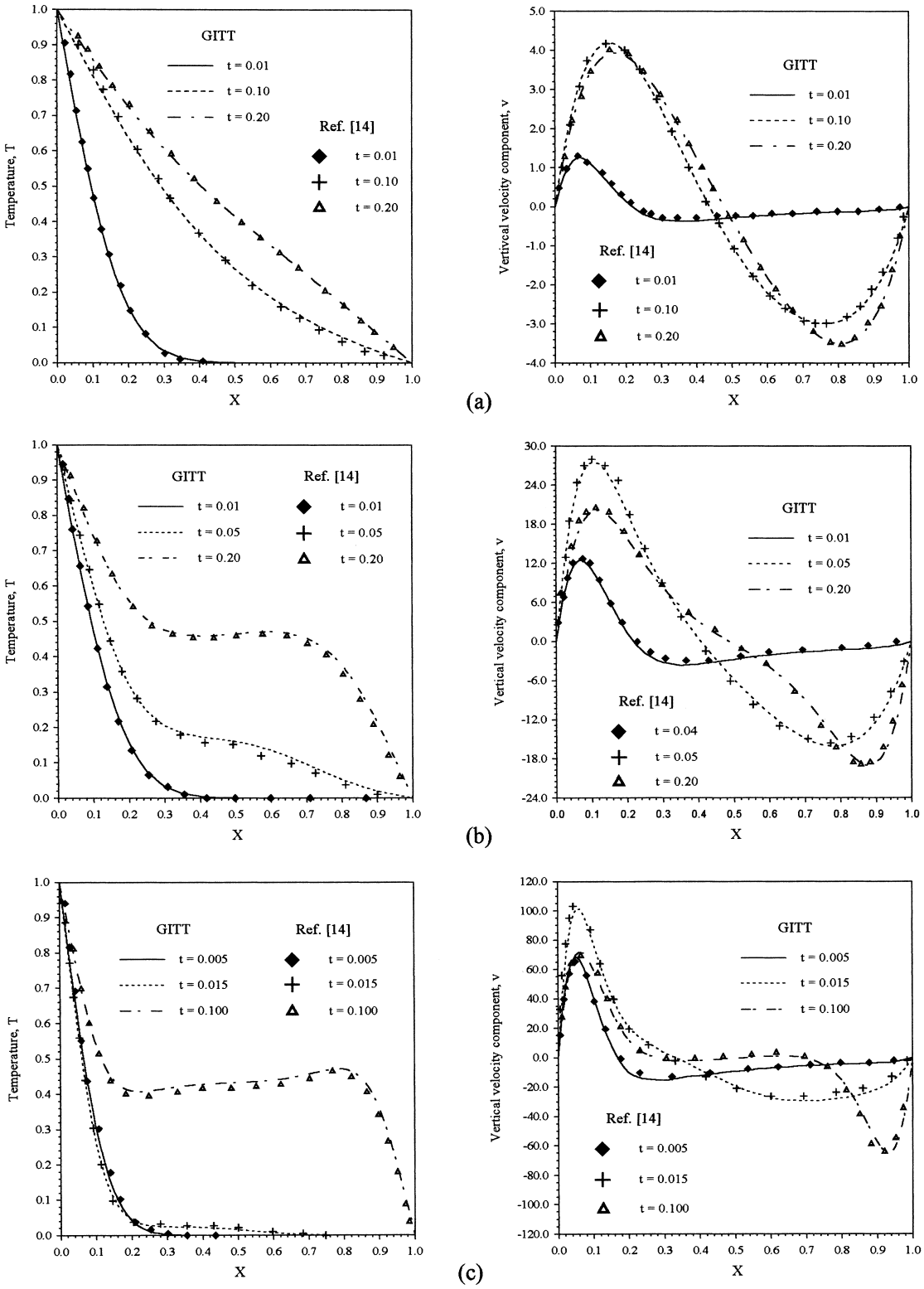

Fig. 1. Temperature and vertical velocity component distributions in the cavity midplane ($y = 1/2$). (a) $Ra = 10^3$, (b) $Ra = 10^4$ and (c) $Ra = 10^5$.

Table 3
Comparison of the stream function at the cavity center, maximum stream function and maximum vertical velocity component for different values of *Ra*, with previous results

Ra	$\lvert\psi_{MED}\rvert$	$\lvert\psi_{MAX}\rvert$	$\lvert V_{MAX}\rvert$
10^3			
GITT — present work	1.175	1.175	3.695
Ramaswamy et al. [15]	1.170	1.175	–
Sai et al. [14]	–	–	3.65
GITT [4] (steady formulation)	1.175	1.175	3.698
De Vahl Davis [7] (steady formulation)	1.174	1.174	3.697
10^4			
GITT — present work	5.073	5.073	19.61
Ramaswamy et al. [15]	5.099	5.099	19.62
Sai et al. [14]	–	–	19.65
GITT [4] (steady formulation)	5.074	5.074	19.63
De Vahl Davis [7] (steady formulation)	5.071	5.071	19.617
10^5			
GITT — present work	9.112	9.614	68.86
Ramaswamy et al. [15]	9.217	9.756	68.62
Sai et al. [14]	–	–	69.50
GITT [4] (steady formulation)	9.116	9.617	68.62
De Vahl Davis [7] (steady formulation)	9.111	9.612	68.59

Table 4
Comparison of the present work steady-state results with some previously reported solutions

Ra	Average Nusselt number along the cavity hot wall				
	GITT (present work)	Finite elements (Sai et al. [14])	Benchmark solution (De Vahl Davis [7])	Estimated deviation with respect to [7] (%)	
				Present work	Sai et al. [14]
10^3	1.118	1.1307	1.117	0.09	1.23
10^4	2.248	2.2894	2.238	0.44	2.30
10^5	4.562	4.6875	4.509	1.18	4.00

ocity component result provided by Sai et al. [14] and De Vahl Davis [7] appears to be more considerable. The computed solutions obtained from the present method, shown in Table 3, indicate a very good agreement when compared with the benchmark solution of De Vahl Davis [7], with a major difference of 0.39% for the vertical velocity component at $Ra = 10^5$ between the present work results and benchmark solutions [7].

Next, quantities of interest in heat transfer calcu-

Table 5
Comparison of the present work with some previously reported benchmark results (steady-state)

Ra	Average Nusselt number along the cavity hot wall			
	GITT (present work)	Benchmark solutions		Estimated deviation with respect to [4,9] (%)
		GITT [4] (steady formulation)	Finite volumes (Hortmann et al. [9])	
10^3	1.118	1.118	–	0
10^4	2.248	2.245	2.245	0.013
10^5	4.562	4.522	4.522	0.885

lations were examined and compared with the finite elements simulation presented in [14], such as the y-averaged Nusselt numbers at the hot wall ($x = 0$) and at the midplane of the cavity ($x = 1/2$), as illustrated in Fig. 2(a)–(c) ($Ra = 10^3$, 10^4 and 10^5). Again, the agreement is very good to the graph scale, including the early stages in the transient behavior, when physical oscillations are expected and obtained. The appearance

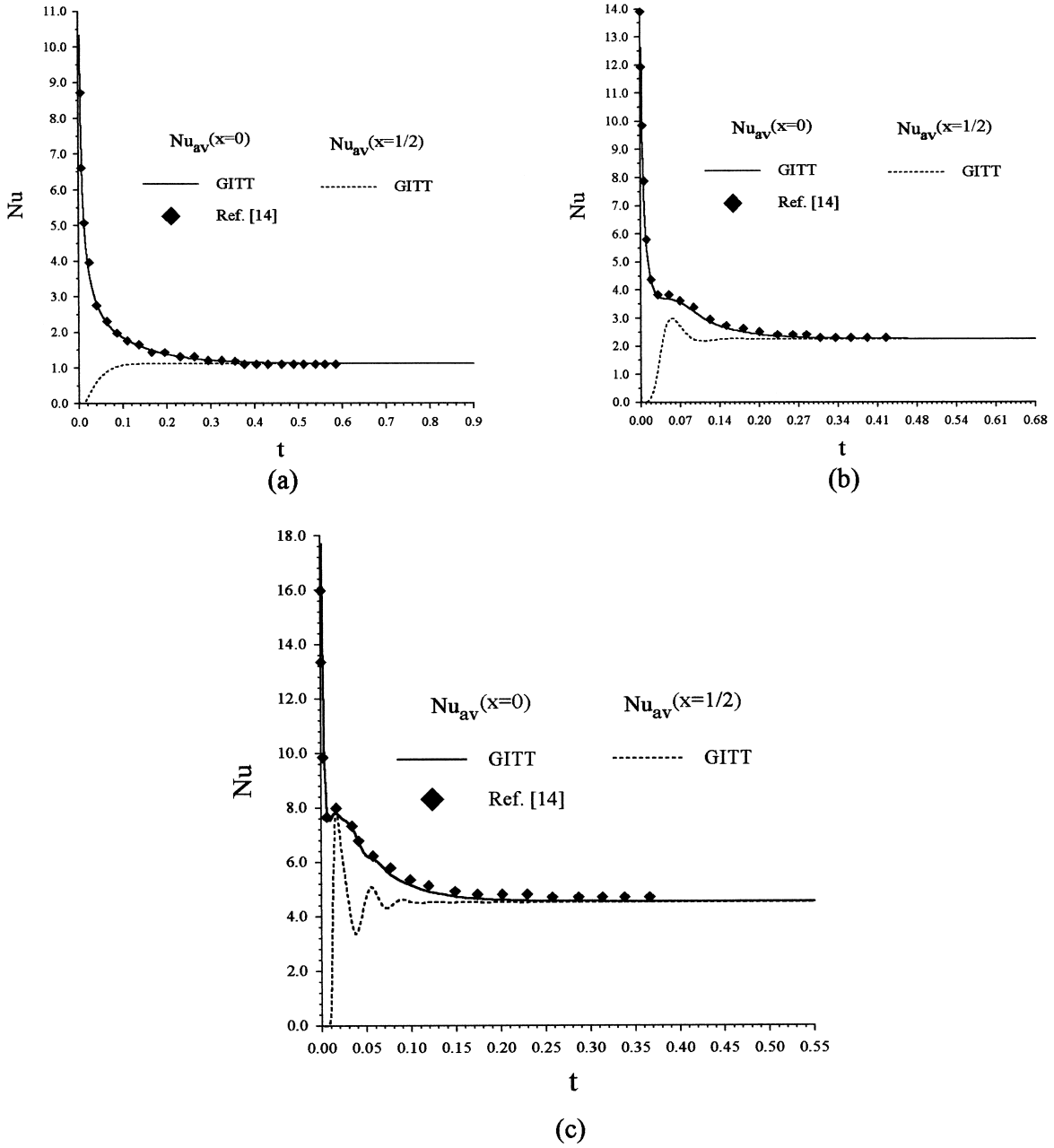

Fig. 2. Development of the average Nusselt number at the hot wall ($x = 0$) and at the cavity vertical midplane ($x = 1/2$) with time. (a) $Ra = 10^3$, (b) $Ra = 10^4$ and (c) $Ra = 10^5$.

of internal waves as Ra is increased is quite noticeable, as can be observed in the oscillations of the average Nusselt number at the cavity midplane evolution.

Tables 4 and 5 illustrate some numerical steady-state values in Boussinesq formulation with constant properties of the y-averaged Nusselt numbers at the hot wall ($x = 0$), $Nu_{av}|_{x=0}$, compared with previously reported solutions. Table 4 presents the estimated relative deviations in percentages for the present work results and for the results of Sai et al. [14], when compared with the classical benchmark solution of De Vahl Davis [7]. Table 5 presents the estimated deviations in terms of percentages for the present work results in relation to two recent benchmark solutions of the steady-state problem, given in [4,9]. Tables 3–5 provide the necessary final confidence on the validation of the developed codes. It can be noticed that the present transient code results for steady-state at high Rayleigh numbers are not fully coincident with the previous GITT simulation for the steady elliptic formulation, since in that situation [4] a single eigenfunction expansion was employed and the resulting coupled boundary value problem could be numerically solved under more strict precision requirements.

Once the present transient code was validated for the constant properties situation, results will be presented for each proposed Rayleigh number, now taking into account the variable properties effects within the three distinct regions planned in Table 1. Thus, the variation of the local Nusselt numbers along the cavity hot wall ($x = 0$) at different times for the three situations are illustrated in Fig. 3(a–c), while the variable properties code, inside the assumed limit of the Boussinesq hypothesis ($\theta_0 = 0.0101$), is compared with the constant properties code.

One can see that for $\theta_0 = 0.0101$, the present variable properties results correspond to those previewed by the Boussinesq hypothesis with constant properties, with a small discrepancy, which is higher at the first value of time shown (0.7% for $Ra = 10^5$). As θ_0 increases, the variable properties effects become more noticeable, and are clearly identified in all three values of Rayleigh number considered. Such behavior is more closely related to the variation of the thermal conductivity, which for the Nusselt number evaluation offers a more direct influence. Fig. 4(a–c) show the evolution of the average Nusselt number at the hot wall against time. Once again, the results for $\theta_0 = 0.0101$ are in good agreement with the constant properties ones. The variable properties effects are observed to be more marked along the flow development, during the time evolution, and less marked on this important averaged quantity as the steady-state situation is approached. The physical oscillations due to the internal waves at higher values of Ra are also significantly altered due to the variable properties consideration.

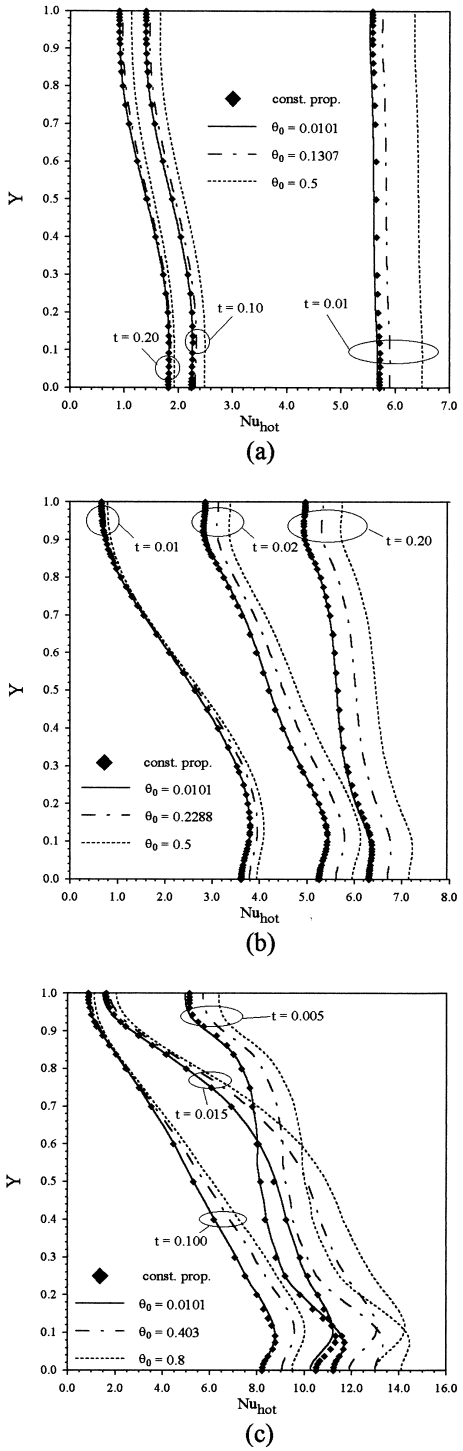

Fig. 3. Comparison of the local Nusselt number along the hot wall of the cavity at different times, for constant and variable properties. (a) $Ra = 10^3$, (b) $Ra = 10^4$ and (c) $Ra = 10^5$.

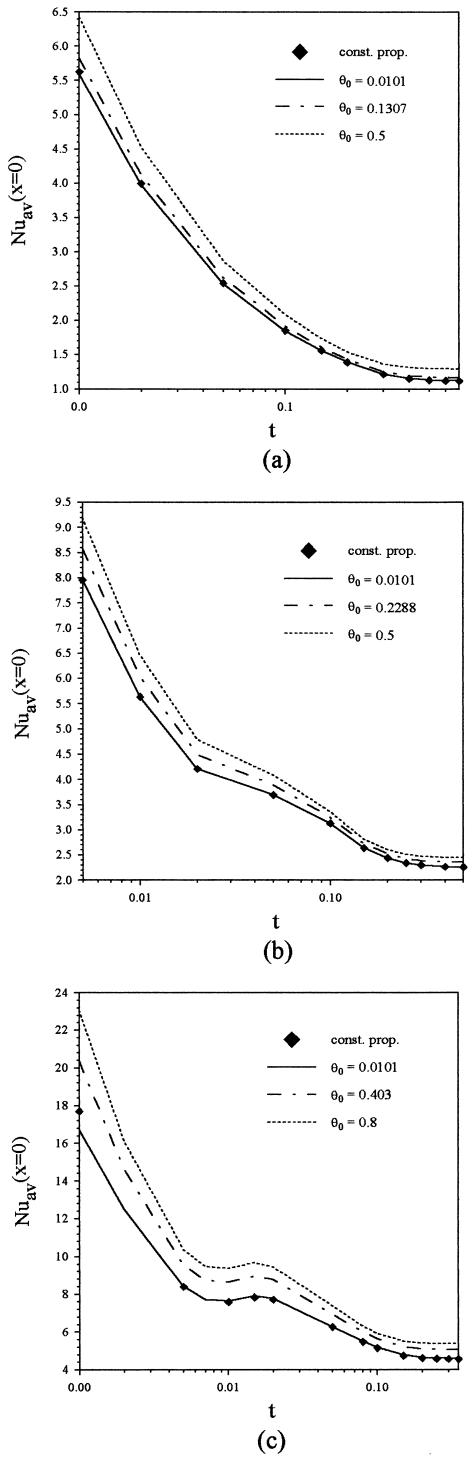

Fig. 4. Variation of the average Nusselt number at the hot wall ($x = 0$), for constant and variable properties. (a) $Ra = 10^3$, (b) $Ra = 10^4$ and (c) $Ra = 10^5$.

Fig. 5(a–d) show the isolines of the streamfunction and temperature for $Ra = 10^5$ for four times of interest. The more noticeable influence of the properties variation in the streamlines seems to be a displacement of the center of circulation, and a reduction of gradients in the x- and y-coordinates. In this case, the main cause of the differences among the curves for each value of θ_0 might be the variation of the viscosity, which more directly affects the rate of momentum exchange. In the isotherms, displacements are also observed, as the heat flux tends to rise in the regions where the convection is expected to be stronger, identified by the increasingly horizontal curves and also clearly observed in the behavior of the Nusselt number variation. The behavior observed in both series of isolines is in accordance to the one found by Suslov [20] and others [18,19], not taking the effects of compressibility into account.

5. Conclusions

Laminar natural convection with variable physical properties inside cavities was successfully solved through the integral transform approach, and critically compared to the constant properties model for different situations defined in relation with theoretical limits for the application of the Boussinesq hypothesis. The computer codes were thoroughly validated against previously reported benchmark solutions, for both steady and transient situations, and used to demonstrate the flexibility of the proposed methodology in dealing with more complex coupled heat and fluid flow models. The Boussinesq approximation was maintained throughout the computations, while varying all the remaining thermophysical properties. It may be concluded that the properties variation effects are considerable even well within the assumed region of applicability for the Boussinesq simplification, as confirmed by the Nusselt number distributions and evolutions, especially along the flow development period. Thus, proposed limits for the density variation simplification are not directly applicable to the properties variation elimination. It may also be observed that limits previewed for the use of the Boussinesq approach might not be totally accurate all along the transient phenomena, though might be acceptable for most steady-state calculations. The present research should now progress towards the removal of the Boussinesq approximation, maintaining the variable properties influence within the transient phenomena, allowing for further and progressive comparisons with the presently reported results.

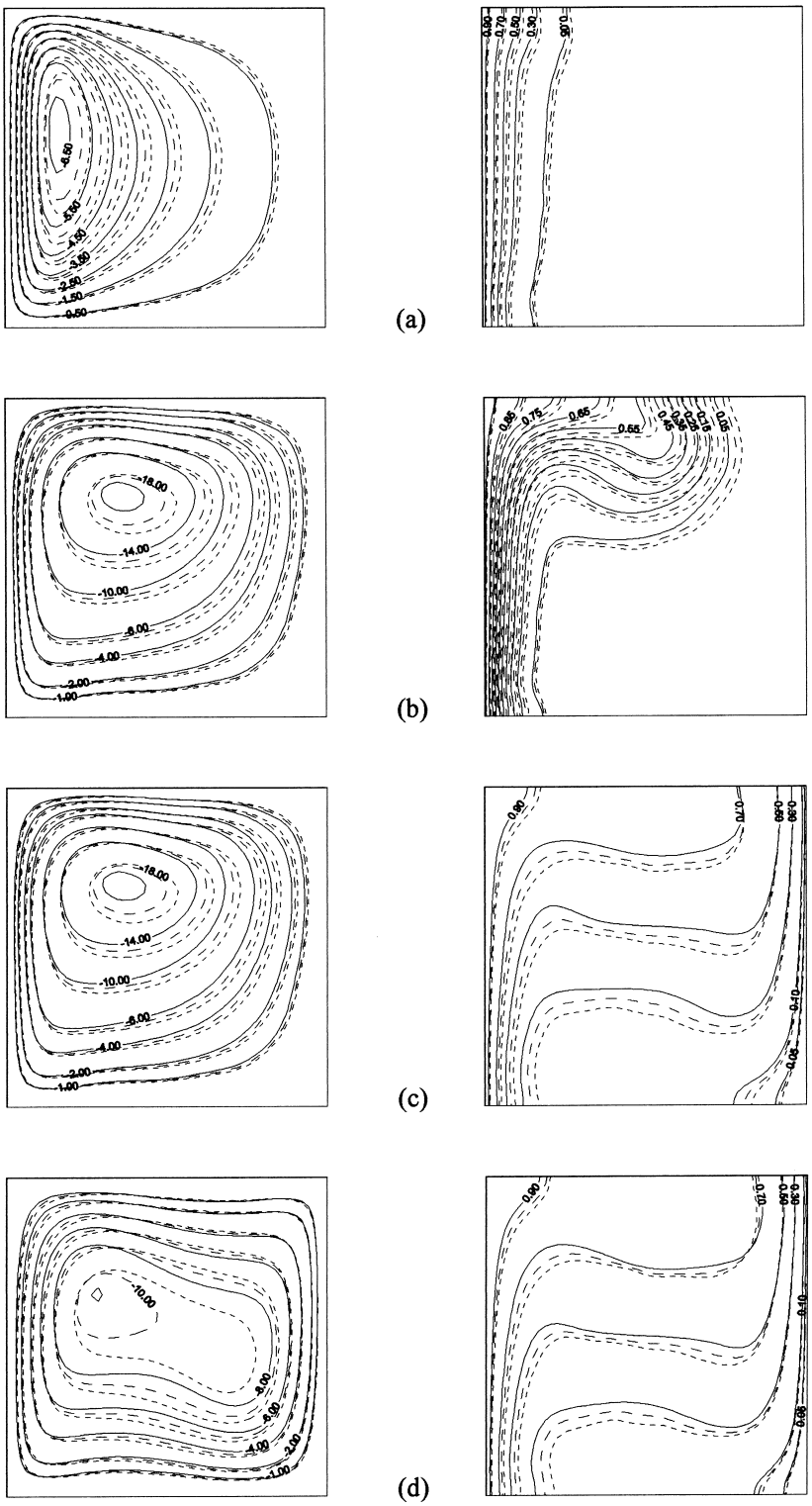

Fig. 5. Streamlines and isotherms for $Ra = 10^5$ at: (a) $t = 0.005$, (b) $t = 0.015$, (c) $t = 0.100$, and (d) $t = 0.550$. (— $\theta_0 = 0.0101$, – – $\theta_0 = 0.403$, - - - $\theta_0 = 0.8$).

Acknowledgements

The authors would like to acknowledge the financial support provided by CNPQ, FUJB, PRONEX and CAPES, federal sponsoring agencies/programs in Brazil.

References

[1] R.M. Cotta, Integral transforms in computational heat and fluid flow, CRC Press, Boca Raton, FL, 1993.
[2] J.S. Pérez Guerrero, R.M. Cotta, Integral transform method for Navier–Stokes equations in streamfunction-only formulation, Int. J. Num. Meth. in Fluids 15 (1992) 399–409.
[3] J.S. Pérez Guerrero, R.M. Cotta, Benchmark integral transform results for flow over a backward-facing step, Comput. Fluids 5 (1996) 527–540.
[4] M.A. Leal, J.S. Pérez Guerrero, R.M. Cotta, Natural convection inside two-dimensional cavities — the integral transform method, Comm. Num. Meth. Eng 15 (1999) 113–125.
[5] M.A. Leal, Natural convection in enclosures, in: R.M. Cotta (Ed.), The Integral Transform Method in Thermal and Fluids Science and Engineering, Begell House Inc, New York, 1998, pp. 375–395.
[6] C. Baohua, R.M. Cotta, Integral transform analysis of natural convection in porous enclosures, Int. J. Num. Meth. in Fluids 17 (1993) 787–801.
[7] G. de Vahl Davis, Natural convection of air in a square cavity: a bench mark numerical solution, Int. J. Num. Meth. in Fluids 3 (1983) 249–264.
[8] T. Saitoh, K. Hirose, High-accuracy bench mark solutions to natural convection in a square cavity, Computational Mechanics 4 (1989) 417–427.
[9] M. Hortmann, M. Peric, G. Scheuerer, Finite volume multigrid prediction of laminar natural convection: bench-mark solutions, Int. J. Num. Meth. in Fluids 11 (1990) 189–207.
[10] P. Le Quéré, Accurate solutions to the square thermally driven cavity at high Rayleigh number, Computers and Fluids 20 (1) (1991) 29–41.
[11] J.O. Wilkes, S.W. Churchill, The finite-difference computation of natural convection in a rectangular enclosure, AIChE J 12 (1966) 161–166.
[12] J. Patterson, J. Imberger, Unsteady natural convection in a rectangular cavity, J. Fluid Mech 100 (1) (1980) 65–86.
[13] A.J. Chorin, A numerical method for solving incompressible viscous flow problems, J. Comp. Physics 2 (1967) 12–26.
[14] B.V.K.S. Sai, K.N. Seetharamu, P.A.A. Narayana, Solution of transient laminar natural convection in a square cavity by an explicit finite element scheme, Num. Heat Transfer, Part A 25 (1994) 593–609.
[15] B. Ramaswamy, T.C. Jue, J.E. Akin, Finite element analysis of oscillatory flow with heat transfer inside a square cavity, AIAA J 30 (2) (1992) 412–422.
[16] A.E. Bergles, Prediction of the effects of temperature dependent fluid properties on laminar heat transfer, in: Fundamentals of Low Reynolds Number Forced Convection, Hemisphere, New York, 1983.
[17] D.D. Gray, A. Giorgini, The validity of the boussinesq approximation for liquids and gases, Int. J. Heat Mass Transfer 19 (1976) 545–551.
[18] E. Graham, Numerical simulation of two-dimensional compressible convection, J. Fluid Mech 70 (4) (1975) 689–703.
[19] L.W. Spradley, S.W. Churchill, Pressure and buoyancy-driven thermal convection in a rectangular enclosure, J. Fluid Mech 70 (1975) 705–720.
[20] S.A. Suslov, S. Paolucci, Stability of natural convection flow in a wall vertical enclosure under non-Boussinesq conditions, Int. J. Heat Mass Transfer 38 (12) (1995) 2143–2157.
[21] S.T. Yu, B.N. Jiang, J. Wu, N.S. Liu, A Div-Curl-Grad formulation for compressible buoyancy flows solved by the least squares finite elements method, Comp. Methods in Applied Mech. and Eng 137 (1996) 59–88.
[22] Z.Y. Zhong, K.T. Yang, J.R. Lloyd, Variable property effects in laminar natural convection in a square enclosure, J. Heat Transfer 107 (1985) 103–138.
[23] S. Wolfram, MATHEMATICA — a system for doing mathematics by computer, in: The Advanced Book Program, Addison-Wesley, Reading, MA, 1991.
[24] M.D. Mikhailov, R.M. Cotta, Ordering rules for double and triple eigenseries in the solution of multidimensional heat and fluid flow problems, Int. Comm. Heat and Mass Transfer 23 (1996) 299–303.
[25] R.M. Cotta, M.D. Mikhailov, Heat Conduction — Lumped Analysis, Integral Transforms, Symbolic Computation, Wiley–Interscience, New York, 1997.
[26] IMSL Library, MATH/LIB, Houston, TX, 1989.
[27] H.A. Machado, M.A. Leal, R.M. Cotta, A flexible algorithm for transient themal convection problems via integral transforms, in: Proc. of the Int. Symp. on Computational Heat and Mass Transfer, Keynote Lecture, North Cyprus, Turkey, 1999, pp. 13–31.